J Polym Eng 32 (2012): 319–326 © 2012 by Walter de Gruyter • Berlin • Boston. DOI 10.1515/polyeng-2011-0135

# Influence of X-ray opaque $BaSO_4$ nanoparticles on the mechanical, thermal and rheological properties of polyoxymethylene nanocomposites

**Issis C. Romero-Ibarra*, Elizabeth Bonilla-Blancas, Antonio Sánchez-Solís and Octavio Manero**

Instituto de Investigaciones en Materiales, Universidad Nacional Autónoma de México, A.P. 70-360, México, D.F., 04510, Mexico, e-mail: issis@unam.mx

*Corresponding author

## Abstract

This work evaluates the influence of a radiopaque reinforcement, barium sulfate ($BaSO_4$), on the mechanical, rheological and thermal properties of polyoxymethylene (POM). Nanocomposites of POM containing spherical nanoparticles of $BaSO_4$ (0, 1, 2, 3 phr) were obtained by melt extrusion in a twin-screw equipment followed by injection molding. The mechanical, thermal and rheological properties of these nanocomposites and the dispersion state of the particles were investigated. Scanning and transmission electron microscopy revealed the morphology of the products. The main objective of this work is the production of nanocomposites with sulfate concentration enough to acquire radiopaque properties while maintaining the mechanical properties of the matrix. In this regard, mechanical and rheological properties were found similar to those of the polymer matrix, but radiopaque contrast tests revealed the influence of the nanoparticles concentration on the optical properties of the composites. The production of these nanocomposites suggests potential applications in the biomedical sector given their unique radio-opacity properties.

**Keywords:** $BaSO_4$; nanocomposites; nanoparticles; polyoxymethylene; radio-opacity.

## 1. Introduction

It is well known that reinforcements, composed of inorganic particles, are widely used in the polymer industry as additives to improve the mechanical, optical or thermal properties of the polymer matrix. When the size of such particles is of the order of nanometers, their high surface energy induces instabilities, such as self-aggregation and a tendency to undertake chemical reactions with the matrix [1].

Polyoxymethylene (POM) is an engineering thermoplastic of the polyacetal type, used to substitute metals or alloys (gears, bushings, etc.) because of its high rigidity, dimensional stability, corrosion resistance, hardness, chemical resistance and good mechanical properties, such as low friction coefficient, low thermal resistance, abrasion resistance and self-lubricating properties [2–7]. However, it lacks high impact and heat resistance, which limits its potential applications [8]. To improve POM properties, blends with inorganic additives have been considered to produce hybrid systems, such as ZnO [2], $MoS_2$ [5], polyhedral oligomeric silsesquioxanes molecules (POSS) and POSS with different organic substituents [6, 7], clays [8, 9], $Al_2O_3$ [4], and nano-$Al_2O_3$/PTFE-$MoS_2$ [10]. Wacharawichanant et al. [2] found that the nanoparticles of ZnO modify POM properties, and thermal degradation of the nanocomposites is increased with ZnO (1.0% wt) content. Xu et al. [9] studied the crystallization kinetics of the POM/montmorillonite blend and found that the crystallization rate was faster than that of the pristine POM. Kongkhlang et al. [8] reported POM/organically modified bentonite, in which the nanocomposite structure is influenced by the surfactant used in the modification of the bentonite. Degradation of POM is accentuated by the organically modified bentonite. Vilà et al. and Sanchéz-Soto et al. produced blends of POM/POSS improving the thermal stability of the POM matrix. This effect has enhanced by the addition of different types of POSS. Good dispersion was achieved upon the addition of amino-functionalized POSS (amino-POSS) that leads to an increase of the thermal decomposition temperature [6] and formation of a more robust polymer/filler network [7]. Although the preparation of nanocomposites of POM mixed with inorganic additives has been reported, a systematic study on the influence of relevant parameters in the synthesis of this nanocomposite is still lacking.

One of the important issues in the nanocomposite preparation is dispersion of the particles to obtain hybrid polymer/inorganic additive systems. Size and distribution of particles in the polymer matrix greatly influence their performance, as well as the processing conditions. In addition, the particle distribution depends on polymer properties, particle size and particle-polymer interactions [11]. Inorganic particles tend to agglomerate and they are immiscible with the polymer matrix [12]. Physical properties (mechanical and optical) of the nanocomposites are largely influenced by particle coalescence into large agglomerates [1, 13], in which the distribution of the opaque particles is poor, resulting in inadequate X-ray opacity [14].

Biomedical applications, such as implants, require that the material be visible under X-rays or fluoroscopy imaging (radiopaque). POM resins have been used in prosthesis since their elastic modulus is similar to that of a bone. Because polymers are not radiopaque, it is necessary to add

a radiopaque element to be visible under X-rays. Types of radiopaque reinforcements used for biomedical applications so far usually affect the quality of the X-ray image, and the mechanical, rheological, thermal and optical properties of the matrix are changed [15, 16]. Barium sulfate ($BaSO_4$) has been used as a reinforcement for polymers and as a radiopaque agent in bones and in dental applications because of its resistance to high temperatures, acids and alkalis [14, 16, 17]. Recently, the blend of POM with micrometric-size particles of $BaSO_4$ was analyzed, although the biological response of the periprosthetic tissue in the presence of the blend was not studied in detail [18]. $BaSO_4$-modified polymer composites have low density, high mechanical properties, low thermal conductivity and are radiopaque to X and UV rays [19]. Hammer and Maurer [20] reported the nucleating effect of $BaSO_4$ in polypropylene (PP), which is improved by incorporating maleic anhydride-grafted PP (PP-g-MAH). The composite PP/$BaSO_4$ showed improved fracture toughness as compared to reference materials. Wang et al. [21, 22] studied the interfacial adhesion control in PP with $BaSO_4$ particles, in which PP was reinforced and showed better hardness. Xu et al. [23] prepared polyvinyl chloride (PVC)/$BaSO_4$ nanocomposites by means of melt-mixing particles. Chen et al. [19] prepared high-density polyethylene HDPE/$BaSO_4$ nanocomposites by melt blending. Previously treated particles of $BaSO_4$ with stearic acid contribute to the uniform dispersion of nano-reinforcements in the matrix, increasing the strength and toughness of the composite.

The addition of nanoscale inorganic particles into the bulk polymer to generate nanocomposites with improved properties relative to the parental materials is a rapidly expanding field [24]. The synthesis, properties and applications of polymer nanocomposites is an interesting area of research. Because of the nanoscale effects and large specific surface area, most of the polymer nanocomposites have special properties in different fields [24, 25]. In particular, the combination of POM polymer and nanoparticles open new perspectives in the application on nanomaterials for biomedical applications with desirable mechanical, thermal and optical properties.

A problem that is usually found when radiopaque and biologically inert $BaSO_4$ particles are added to the polymer is the loss of ductility and flexibility of the resulting products, especially when the size of these particles is in the micron range, due to the relatively large concentrations needed for radio-opacity. One of the objectives of this work is the production of nanocomposites by careful synthesis of particles in the nanoscale range to achieve two important goals: an adequate level of radio-opacity while maintaining the mechanical, rheological and thermal properties of POM, using relatively small $BaSO_4$ (0, 1, 2, 3 phr) concentrations. $BaSO_4$ nanoparticles were synthesized in presence of the capping agent ethylenediaminetetraacetic acid (EDTA). This modifier can direct the nucleation and growth of the nanoparticles' spherical shape. Qualitative studies of optical contrast under X-rays revealed potential applications in the biomedical industrial sector.

## 2. Experimental

### 2.1. Materials

The polymer matrix is POM, homopolymer, Delrin II 150SA NC010 from DuPont (México, D.F., México) obtained in pellets. POM (-$[CH_2$-$O]_n$-) is synthesized from formaldehyde or trioxymethylene through cationic polymerization [3].

Nanoparticles of $BaSO_4$ were prepared through a precipitation reaction *in situ* in aqueous medium. Solutions of $BaCl_2 \cdot 2H_2O$ (Baker, 99.9%) and $Na_2SO_4$ (Baker, 99%) were mixed in the presence of disodium EDTA-2Na·$2H_2O$ (Baker, 99.9%) at ambient temperature. This process generated 50-nm-size particles, in agglomerates with mean diameter of 500 nm (secondary particles). Romero-Ibarra et al. [26] reported the influence of the synthesis conditions on the nanoparticles' morphology.

Degradation was controlled during the extrusion process using an antifoam agent, silicone-based A-289 (Aldrich, México, D.F., México, 99.9%).

### 2.2. Equipment

The processing of the ingredients was carried out in a Haake Rheocord 90 TW-100 twin-screw counter-rotating extruder with a length of 331 mm and L/D ratio of 27. Samples for mechanical tests were molded in a Mannesman Demag Ergotech 50-200 injection molding machine with L/D=20.

The particle dispersion analysis was carried out in a scanning electron microscope (SEM) Leica Stereoscan 440. The gold-coating conducting layer was provided by a Fine Coat Ion-Sputter JFC-110 Jeol equipment. Specimens were previously fractured with liquid nitrogen. The size and morphology of the nanocomposites were characterized by a transmission electron microscope (TEM) Carl Zeiss EM910 with an acceleration voltage of 120 kV. Samples for tension tests were previously fractured and cut into thin layers (~70 nm) using an ultramicrotome equipped with diamond blades in liquid nitrogen.

Mechanical tests were done in an Instron machine 1125 under a constant strain rate of 50 mm/min, according to the ASTM D 638-91 norm. Impact test was performed following ASTM-D 256 Izod-notched type.

Thermal analyses (thermogravimetric, TGA, and differential scanning calorimetry, DSC) were performed in a TA Advanced Universal Analysis 2000 Instruments SDT600. Samples were placed in aluminum vials with a flow of 100 ml/min under nitrogen atmosphere with a heating rate of 10°C/min. $T_{descomp}$ is obtained from the slope change and inflection point of the TGA thermogram, where the maximum degradation occurs. $T_{5\%}$ is the data of the weight loss at 5% and $T_{max}$ is the maximum weight loss rate. The melting temperature and enthalpies ($\Delta H$) were determined from the maxima and the areas of the corresponding peaks, respectively. The crystalline percentage of the nanocomposites was obtained following the relation $\Delta H_f/\Delta H^\circ_f$ theoretical×100. The theoretical $\Delta H^\circ_f$ of the POM homopolymer is 326.3 J/g [27].

Rheological characterization was performed in a TA Instruments AR 1000-N stress-controlled rheometer with parallel plates of 25 mm diameter at 190°C.

Radio-opacity tests were determined following the ASTM F640-79 standard. Images were taken with the clinical-standard X-ray equipment CMR MRH-II operated at 300 mA and 50 kV with a tungsten bulb of 100 mA at 0.02 s.

### 2.3. Nanocomposite preparation

$BaSO_4$ nanoparticles were mixed with the polymer pellets and processed at 25 rpm in the extruder. The product was injection-molded to obtain samples for mechanical tests. Extrusion temperature profile was 190–190–190–185°C and that of the injection process was 220–210–210–200°C. The antifoam agent was added at 0.5 wt% concentration during extrusion. All raw materials were previously dried. Sample description is shown in Table 1.

## 3. Results and discussion

### 3.1. Morphology

$BaSO_4$ particles were obtained in the presence of EDTA and they are shown in Figure 1. The morphology of the spherical particles is shown in the inset. Diameters of the agglomerates (secondary particles) ~500 nm are conformed by smaller particles ~50 nm. These aggregates of ~50 nm are themselves formed by smaller nanoparticles of ~4 nm, as demonstrated in a previous study [26]. The particles were mixed with POM subsequently.

Figure 2 shows the micrographs of pristine POM and POM with 1 phr $BaSO_4$ nanoparticles in the presence and absence of the antifoam agent, respectively. In Figure 2A, the polymer presents a smooth-fractured surface. Figure 2B exhibits the fracture surface of an extruded thread with 1phr $BaSO_4$ particles, in which foaming was present. It is likely that $BaSO_4$ and the processing of the material generate formaldehyde vapors that produce bubbles and pores (see inset in Figure 2B). When the blend is prepared without the antifoam agent (Figure 2B), a material with trapped bubbles is obtained. This material tends to degrade under the thermo-mechanical processing and the resulting product has low mechanical properties [28]. Note that POM tends to degrade under thermal processes, resulting in several side products such as carbon dioxide, carbon monoxide and formaldehyde. These species are originated from depolymerization reactions of the terminal chains and random rupture of oxymethylene chains [8].

**Table 1** POM/$BaSO_4$ nanocomposite formulations.

| Sample | Agent | Formulation |
|---|---|---|
| POM | – | POM extruded+0.5% antifoam |
| POM/$BaSO_4$-1 | EDTA | POM+1 phr nano $BaSO_4$ spherical agglomerate+0.5% antifoam |
| POM/$BaSO_4$-2 | EDTA | POM+2 phr nano $BaSO_4$ spherical agglomerate+0.5% antifoam |
| POM/$BaSO_4$-3 | EDTA | POM+3 phr nano $BaSO_4$ spherical agglomerate+0.5% antifoam |

The fracture surfaces correspond to those of a brittle material, presenting high porosity resulting in low mechanical, rheological and optical properties. Lu et al. [29] reported polymer foaming and degradation during processing of $BaSO_4$-filled medical-grade thermoplastic polyurethane system. The addition of the antifoam agent controls the degradation and bubble generation as the $BaSO_4$ particles are incorporated (Figure 2C). The SEM image of the POM/$BaSO_4$-1 blend exhibits uniform particle distribution and dispersion.

Figure 3A–C shows SEM and TEM images of the POM+1 phr $BaSO_4$ blend, where it is clearly apparent that barium sulfate particles are embedded in the POM matrix. In Figure 3A, slightly agglomerated particles with size of ~1 μm are formed during the extrusion process. In Figure 3B, particle agglomerates of ~50–500 nm are observed. The TEM image in Figure 3C shows an amplification confirming that the agglomerates are formed themselves with primary particles with smaller sizes in the nanometric scale (~4 nm, as determined in Ref. [26]). Secondary particles are deformed by shear stresses under processing.

As observed in the previous images, a material with good particle dispersion and uniform distribution was obtained with sizes in the nanoscale. It is well known that if the particles are not well dispersed, these are likely to be nucleating sites where microfractures may initiate. The absence of micrometer-size aggregates is indicative of a high level of miscibility or compatibility between the POM matrix and the particles [7]. The particle synthesis and processing conditions for the blend must overcome the natural tendency of particles to agglomerate, which makes particle dispersion difficult [30]. $BaSO_4$ particle dispersion depends also on the functional groups of the polymer matrix and additional compounds. A stabilizing agent during the particle synthesis, such as EDTA, helps in controlling particle size and agglomeration rate reduction, as observed in Figure 3B and C.

### 3.2. Mechanical properties

Table 2 shows some of the mechanical test results, comparing data of pristine POM with those of the extruded

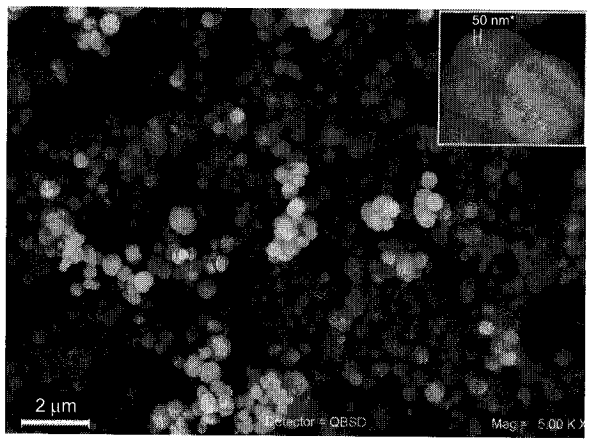


**Figure 1** SEM images of the $BaSO_4$ nanoparticles.


**Figure 2** SEM images of (A) POM+antifoam, (B) POM+1 phr de $BaSO_4$ (without antifoam) and (C) POM+1 phr de $BaSO_4$+antifoam.

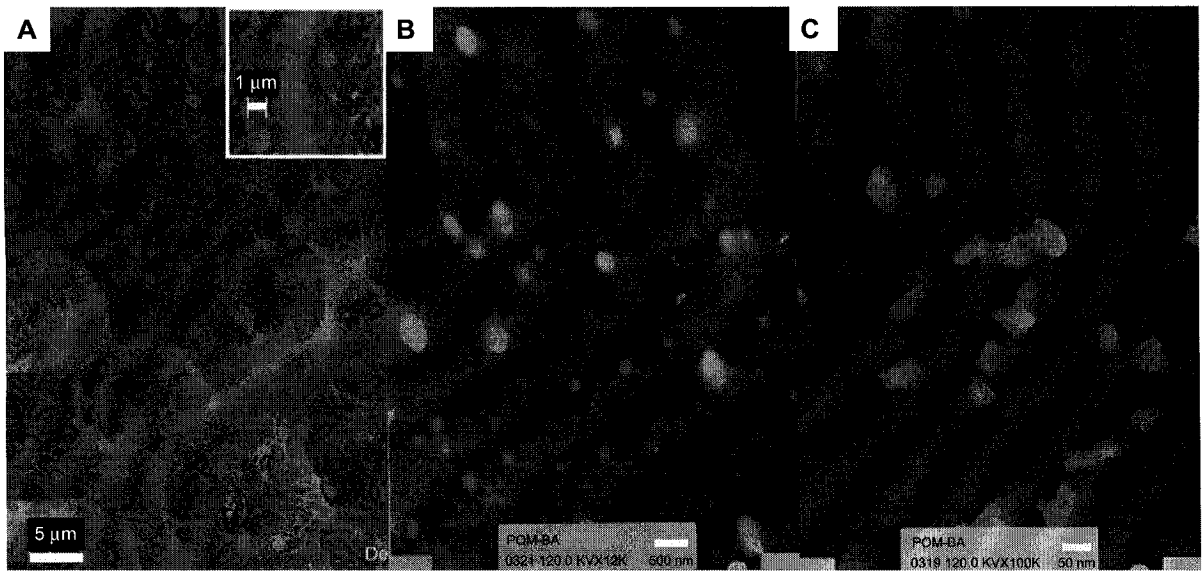


**Figure 3** POM with 1 phr $BaSO_4$ nanoparticles. (A) SEM image, (B) TEM image and (C) amplified TEM image.

nanocomposites. All systems were prepared with the same thermomechanical history.

In general, the introduction of 1 phr $BaSO_4$ nanoparticles does not substantially modify the mechanical properties of the matrix, whereas these are diminished upon increasing $BaSO_4$ content to 3 phr.

An increase in the strain at break of 13.5% is measured in the sample of 1 phr $BaSO_4$ (POM/$BaSO_4$-1). However, this value is not significant because is in the range of the experimental uncertainties. For larger $BaSO_4$ contents (2 phr) mechanical properties are maintained at the level of the matrix, although they diminish as compared to data of the system with 1 phr. With 3 phr, a definite decrease in the mechanical properties is apparent. Strain at break is lower, possibly due to degradation and poor dispersion at these high particle contents. Attractive forces overcome dispersion forces, which leads to agglomeration and reduced dispersion and distribution of particles in the polymer matrix. Agglomerates act as stress concentrators that presumably are potential sites for fracture propagation. In particular, the system POM/$BaSO_4$ did not interact substantially with the POM matrix, as no detectable FTIR bands are recorded (data not shown). In summary, mechanical properties are slightly affected at high particle concentrations; notwithstanding, the system with 1 phr particle content fulfills expectations related to biomedical applications. Indeed, the applications sought in the field of polymer biomedical devices do not need large increases in their mechanical properties.

**Table 2** Mechanical properties of the systems.

| Formulation | Tensile stress (MPa) | Strain at break (%) | Young modulus (MPa) | Impact strength (J/m) |
|---|---|---|---|---|
| POM | 69±4 | 37±5 | 1383±15 | 492±3 |
| POM/$BaSO_4$-1 | 70±2 | 42±7 | 1378±16 | 478±7 |
| POM/$BaSO_4$-2 | 62±2 | 34±5 | 1298±14 | 507±3 |
| POM/$BaSO_4$-3 | 62±2 | 23±4 | 1255±20 | 474±7 |

### 3.3. Thermal properties

Figure 4 illustrates thermogravimetric curves of POM and POM/$BaSO_4$ nanocomposites. Extrusion was carried out at 190°C, at which there is no appreciable weight loss. At 261°C

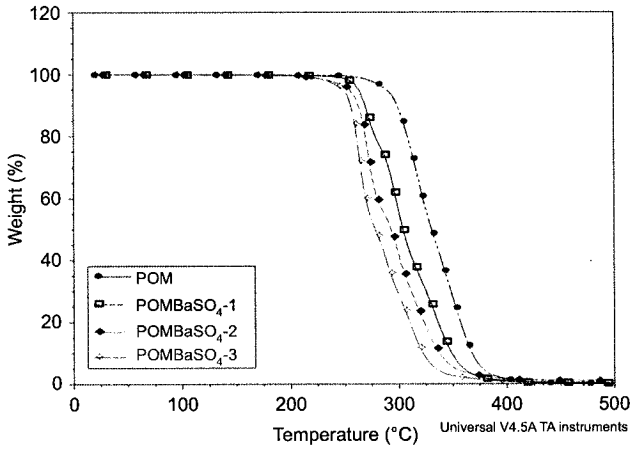


**Figure 4** TGA curves under nitrogen with heating rate of 10°C/min for (A) POM, (B) POM/$BaSO_4$-1 (C) POM/$BaSO_4$-2 and (D) POM/$BaSO_4$-3.

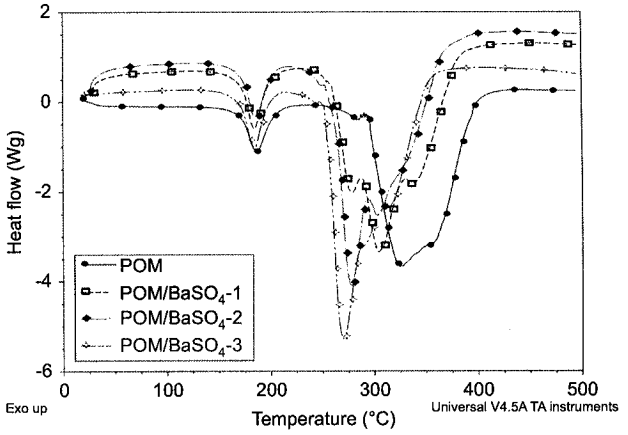


**Figure 6** DSC curves under nitrogen with heating rate of 10°C/min for (A) POM, (B) POM/$BaSO_4$-1 (C) POM/$BaSO_4$-2 and (D) POM/$BaSO_4$-3.

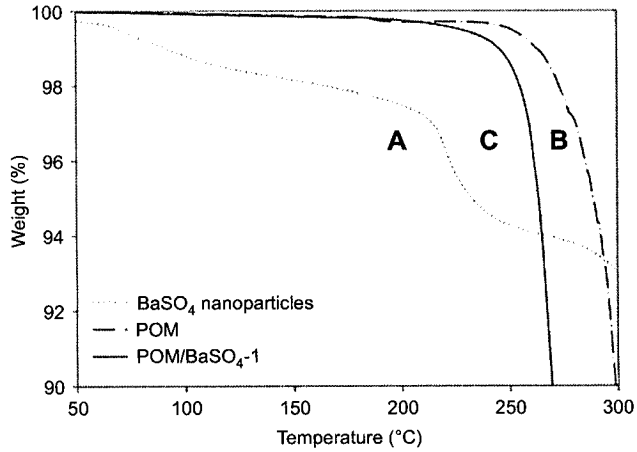


**Figure 5** TGA: high resolution for (A) $BaSO_4$ nanoparticles, (B) POM and (C) POM/$BaSO_4$-1.

the weight loss is ~1% in POM, and 3.9%, 8.6% and 19.9% for the blends with 1, 2, and 3 phr of $BaSO_4$, respectively. In general, larger weight losses are measured upon increasing temperature and $BaSO_4$ content (e.g., at 300°C, weight loss is 14% for POM and 42%, 60% and 72% for 1, 2, and 3 phr, respectively). As the concentration of $BaSO_4$ increases, the trend for particle agglomeration is more apparent, and thermal stability tends to diminish. With 3 phr $BaSO_4$, thermal stability decreases, revealing that, in general, thermal stability of the POM/$BaSO_4$ nanocomposites is closely related to $BaSO_4$ content and agglomerate concentration.

Figure 5 corresponds to the high-resolution TGA of the (A) $BaSO_4$ nanoparticles, (B) POM and (C) POM mixed with 1 phr of $BaSO_4$. It shows that the thermal stability of the nanocomposite decreased slightly when particles are incorporated. The interval from 210°C to 300°C coincides with the EDTA weight loss of the nanoparticles. Within the EDTA decomposition interval (246–275°C), the calculated EDTA concentration adsorbed at the surface of the $BaSO_4$ nanoparticles is 0.7%. However, no large effects on the thermal stability are measured at the required processing temperature range (185–220°C).

Data of the temperature at 5 wt.% weight loss ($T_{5\%}$) and that of the maximum weight loss ($T_{max}$) [7] for neat POM and POM/$BaSO_4$ composites (1, 2, 3 phr of $BaSO_4$) are presented in Table 3. For the neat POM, these values are $T_{5\%}$ of 288.4°C and $T_{max}$ of 318.4°C, whereas both parameters diminished with the increase of $BaSO_4$ concentration in the nanocomposites. In the range of processing temperatures the samples are stable upon introduction of the $BaSO_4$ particles.

DSC data for nanocomposites are depicted in Figure 6, and Table 3 shows the information gathered from the thermograms.

Table 3 indicates lower thermal stability of the nanocomposites upon increasing temperature with respect to that of neat POM. According to this lower thermal stability, melting

**Table 3** Data obtained from TGA and DSC thermograms for the POM/$BaSO_4$ systems.

| Sample | TGA | | DSC | | | | |
|---|---|---|---|---|---|---|---|
| | $T_{5\%}$ (°C) | $T_{max}$ (°C) | $T_m$ (°C) | $\Delta H_m$ (J/g) | Crystallinity (%) | $T_{decomp}$ (°C) | $\Delta H_{decomp}$ (J/g) |
| POM | 288.4 | 318.4 | 187.0 | 134 | 41.1 | 324.1 | 1430 |
| POM/$BaSO_4$-1 | 265.1 | 297.6 | 184.5 | 148 | 45.4 | 304.5 | 1773 |
| POM/$BaSO_4$-2 | 254.4 | 271.1 | 185.9 | 143 | 43.8 | 260.0 | 1825 |
| POM/$BaSO_4$-3 | 248.1 | 263.1 | 184.5 | 145 | 44.4 | 254.6 | 1576 |

temperature diminishes with increasing particle content. This result is attributed to size and distribution of the microcrystallites of POM in POM/$BaSO_4$, which are smaller and with broader distribution than those of pure POM. Degradation temperature decreases drastically with increasing $BaSO_4$ content, and the change is more accentuated between 1 and 2 phr. The minimum in the decomposition temperature occurs at 2 phr, coinciding with the maximum in the decomposition enthalpy, which decreases steeply between 2 and 3 phr. Nanocomposite degradation temperature may also be affected by EDTA presence since Ba-EDTA degradation temperature is ~250°C [31] (see Figure 5). Therefore, the degradation of POM might be attributed to a POM chain scission and depolymerization due to the presence of EDTA.

$\Delta H$ values of the nanocomposites are larger than those of pure POM, indicating larger crystallinity with increasing particle content. Similar results were obtained by Qu et al. [12] and Yao and Yang [13], although these values are within the experimental uncertainties. In the POM/$BaSO_4$ system, upon increasing the nanoparticle content, particles tend to aggregate, discouraging the nucleating effect. The melting temperature and the crystallinity level of POM remained practically constant, indicating that the crystalline structure of POM is not affected upon the addition of $BaSO_4$.

As shown in Figure 7, in the SEM image of pure POM mixed with EDTA, the degradation of the polymer matrix is apparent as pores and a brittle surface appear. The EDTA adsorbed on the $BaSO_4$ surface has a sufficiently low concentration (0.7 wt.%) to maintain the properties of the blend with 1 phr $BaSO_4$. However, upon increasing particle concentration, the EDTA content on the particle surface also increases. In this form, the stabilizing agent used in the nanoparticle synthesis may influence the thermal decomposition of the nanocomposite to levels lower than those of the precursor polymer. Therefore, a critical concentration of the stabilizer is suggested, above which chain rupture and degradation are catalyzed by EDTA.

The DSC data (Figure 6) reveal the initiation of melting at ~184°C for the nanocomposites, followed by an endothermic peak previous to decomposition. As particle content increases (3 phr), the peak is more accentuated, may be due to the nucleating properties of $BaSO_4$. Reports on the modification of rate of crystallization by nucleation (and crystal size) and thermal behavior of the polymers are available [2, 12, 32, 33].

In summary, blends are thermally stable within the temperature range of the extrusion and molding processes (185–210°C). The melting temperature and the cristallinity level of POM remained practically constant, indicating that the crystalline structure of POM is not affected negatively upon the addition of $BaSO_4$. The thermal degradation of POM is thought to be due to chain scission of the C-O-C bonds [7]. Upon increasing particle content at temperatures higher than 240°C, a major weight loss is measured and thermal degradation occurs, attributed to polymer chain scission, agglomerate formation and EDTA content (decomposition initiates at ~250°C).

### 3.4. Rheological properties

Figure 8 describes a plot of shear viscosity as a function of shear rate for POM and the nanocomposites formed by spherical particles.

All samples tend to similar zero shear-rate viscosity for low shear rates, whereas for larger shear rates, shear thinning occurs. POM and POM with 1 phr $BaSO_4$ exhibit similar values, with the nanocomposite attaining the larger viscosity. The decrease in viscosity with increasing shear rate is more gradual than that of the nanocomposites with larger particle concentration. Indeed, for the larger particle contents, the decrease in viscosity is very steep, approaching the slope of -1.

The viscosity measured in the nanocomposite with 1 phr particle content reveals strong polymer-particle interactions [34]. It is likely that the first stage with gradual shear thinning is due to flow-induced chain disentanglement and lubrication of shear surfaces by the presence of the particles [35]. However, the second more pronounced slope change is not due to a rheological mechanism but to initial degradation of the polymer matrix during processing. Notice that the slope change is more gradual when particle

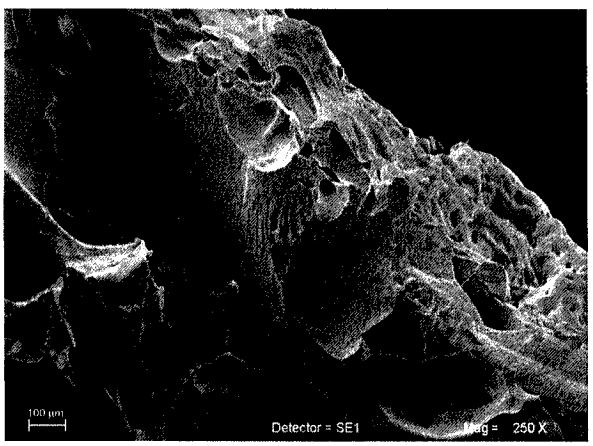


**Figure 7** Extruded POM with EDTA.

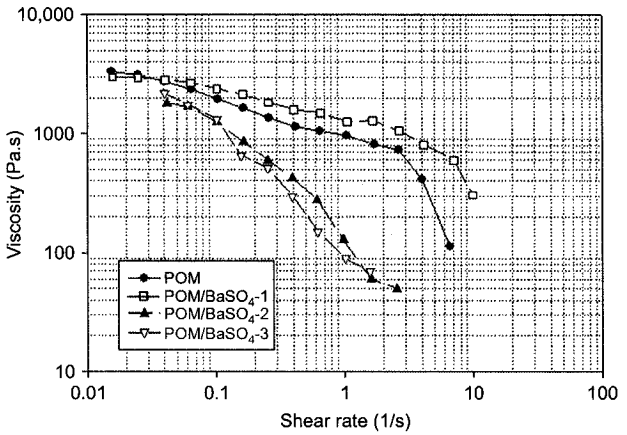


**Figure 8** Shear viscosity as a function of shear rate for the four systems studied.

*content is 1 phr, manifesting higher polymer-particle structural stability.*

With particle contents of 2 and 3 phr $BaSO_4$, the structure breakage associated with such pronounced shear thinning is quite possibly due to thermal degradation, as discussed in the thermal properties of these systems.

The complex viscosity (not shown) presents similar behavior in both POM and the nanocomposite with 1 phr $BaSO_4$; this agrees with results by Lai et al. [35].

Figure 9 presents the modulus (storage and loss) *versus* frequency for POM and nanocomposite with 1 phr particle concentration. The loss modulus of both the POM and nanocomposite has similar values within three decades of behavior, slightly less in the nanocomposite. The storage modulus exhibits larger differences. It is substantially larger in POM as compared to that of the nanocomposite. Nonetheless, in the low-frequency extreme, the trend reverses. $G'$ of the nanocomposite has a tendency to level off, attaining slightly larger values than $G'$ of pure POM. This behavior is characteristic of the formation of an elastic network brought about by high polymer-particle interactions [8, 36]. As the slope tends to zero, a near solid-like behavior reveals not only augmented particle-polymer interactions but also that the limiting slope is a criterion of the degree of dispersion of particles in the polymer matrix [37–39].

### 3.5. Radio-opacity

In Figure 10, X-ray radiographs of the nanocomposites are exposed. Figure 10A shows the more intense contrast corresponds to the one with the largest particle content (3 phr). Figure 10B and 10C have 2 and 1 phr $BaSO_4$, respectively. With respect to the optimum $BaSO_4$ concentration for radio-opacity, two important factors need to be taken into account: the level of radio-opacity and mechanical properties. Very large amounts of $BaSO_4$ particles induce agglomeration and poor mechanical properties, and the system is not easily extruded or molded. The optical properties (visibility of the sample under X-ray or fluoroscopic imaging) are affected by numerous factors, and hence the amount of radiopaque agent for better radiographies depends directly on the type of application.

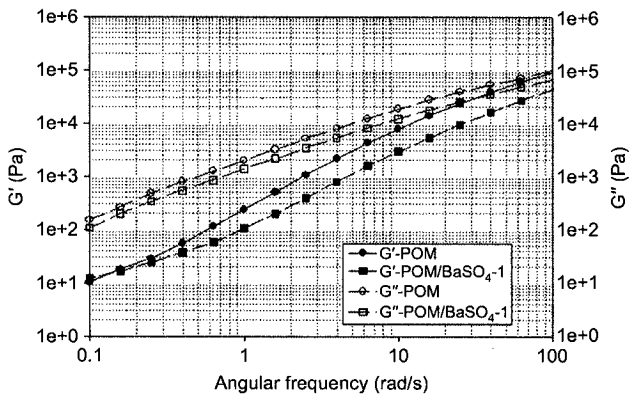


**Figure 9** Storage modulus ($G'$) and loss modulus ($G''$) as functions of angular frequency for POM and POM/ $BaSO_4$ with 1 phr particle concentration.

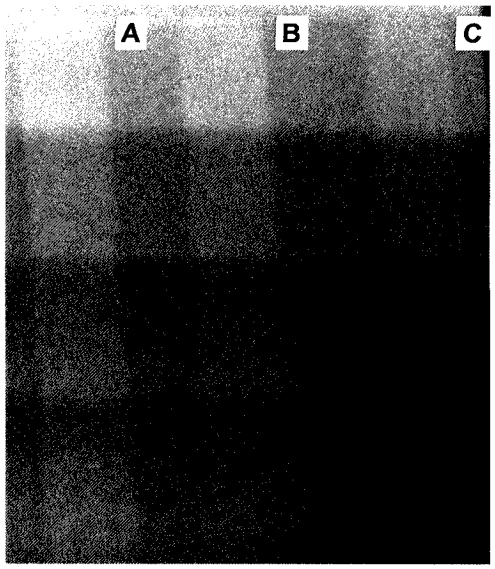


**Figure 10** Radiography of mold-injected samples of the nanocomposites with variable amounts of $BaSO_4$. (A) POM/$BaSO_4$-3 (B) POM/$BaSO_4$-2 and (C) POM/$BaSO_4$-1.

## 4. Conclusions

In this work, spherical nanoparticles of barium sulfate were dispersed in the POM matrix. SEM and TEM images show evidence of the dispersion and distribution of the particles in the polymer at 1 phr of concentration.

The introduction of a stabilizing agent during the synthesis, EDTA, allows controlling the particle size and rate of agglomeration. The nanocomposites produced were characterized, exhibiting mechanical and rheological properties similar to those of the polymer, but with added radio-opacity properties. In general, the nanocomposites do not exhibit a negative influence upon the original properties of the polymer matrix, which constitutes one of the objectives of this work. The systems are thermally stable within the processing conditions. Radio-opacity to X-ray tests revealed an increase in the optical contrast as the $BaSO_4$ concentration increases, allowing the control of the optical density. A compromise exists in the balance between mechanical and optical properties with regard to products intended for biomedical applications.

## Acknowledgements

I.C. Romero-Ibarra thanks the CONACyT for the scholarship (no. 181930) and the PAPIIT UNAM project IN-116510/22. The authors acknowledge the contributions from O. Novelo, C. Flores, E. Fregoso, F. Calderas, R. Cedillo and I. Vazquez in the SEM, TEM, thermal analysis, rheological measurements and radio-opacity determinations, respectively. M.F. García-Sánchez is also acknowledged for the fruitful discussions.

## References


[1] Rozenberg BA, Tenne R. *Prog. Polym. Sci.* 2008, 33, 40–112.
[2] Wacharawichanant S, Thongyai S, Phutthaphan A, Eiamsamang C. *Polym. Test.* 2008, 27, 971–976.
[3] Li Y, Zhou T, Chen Z, Hui J, Li L, Zhang A. *Polymer* 2011, 52, 2059–2069.
[4] Sun L-H, Yang Z-G, Li X-H. *Wear* 2008, 264, 693–700.
[5] Hu KH, Wang J, Schraube S, Xu YF, Hu XG, Stengler R. *Wear* 2009, 266, 1198–1207.
[6] Vilà N, Sánchez-Soto M, Illescas S. *Polym. Comp.* 2011, 32, 1584–1592.
[7] Sánchez-Soto M, Illescas S, Milliman H, Schiraldi D, Arostegui A. *Macrom. Mat. Eng.* 2010, 295, 846–858.
[8] Kongkhlang T, Kousaka Y, Umemura T, Nakaya D, Thuamthong W, Pattamamongkolchai Y, Chirachanchai S. *Polymer* 2008, 49, 676–1684.
[9] Xu W, Ge M, He P. *J. Appl. Polym. Sci.* 2001, 82, 2281–2289.
[10] Sun L-H, Yang Z-G, Li X-H. *Polym. Eng. Sci.* 2008 48, 1824–1832.
[11] Che J, Xiao Y, Wang X, Pan A, Yuan W, Wu X. *Surf. Coat. Tech.* 2007, 201, 4578–4584.
[12] Qu MH, Wang YZ, Wang C, Ge XG, Wang DY, Zhou Q. *Euro. Polym. Jnl.* 2005, 41, 2569–2574.
[13] Yao C, Yang G. *Polym. Adv. Technol.* 2009, 20, 768–774.
[14] Davy KW, Anseau MR, Odlyha M, Foster GM. *Polym. Int.* 1997, 43, 143–154.
[15] Ramakrishna S, Mayer J, Wintermantel E, Leong KW. *Compos. Sci. Technol.* 2001, 61, 1189–1224.
[16] Guo X. *J. Appl. Polym. Sci.* 2008, 109, 4015–4024.
[17] Nuutinen J-P, Clerc C, Törmälä P. *J. Biomater. Sci. Polymer. Edn.* 2003, 14, 665–676.
[18] Stražar K, Kavčič M, Simčič J, Pelicon P, Šmit Ž, Kump P, Jaćimović R, Antolič V, Cör A. *Nucl. Instr. Meth. Phys. Res. B.* 2006, 249, 719–722.
[19] Chen X, Wang L, Liu Y, Shi J, Shi H. *Polym. Eng. Sci.* 2009, 49, 2342–2349.
[20] Hammer CO, Maurer FHJ. *Polym. Eng. Sci.* 1998, 38, 1295–1302.
[21] Wang K, Wu J, Zeng H. *Euro. Polym. Jnl.* 2003, 39, 1647–1652.
[22] Wang K, Wu J, Ye L, Zeng H. *Composites Part A* 2003, 34, 1199–1205.
[23] Xu Y, Zhang XZ, Zhou CX, Wu WS, Shi LY, Yang B. *Polym. Mater. Sci. Eng.* 2007, 23, 144.
[24] Luan J, Wang S, Hu Z, Zhang L. *Curr. Org. Synth.* 2012, 9, 114–136.
[25] Osman AF, Edwards GA, Schiller TL, Andriani Y, Jack KS, Morrow IC, Halley PJ, Martin DJ. *Macromolecules* 2012, 45, 198–210.
[26] Romero-Ibarra IC, Rodríguez-Gattorno G, García-Sánchez MF, Sánchez-Solís A, Manero O. *Langmuir* 2010, 26, 6954–6959.
[27] Martins JA, Cruz Pinto JJC. *Polymer* 2002, 43, 3999–4010.
[28] Archodoulaki VM, Lüftl S, Seidler S. *Polym. Test.* 2006, 25, 83–90.
[29] Lu G, Kaylon DM, Yilgör I, Yilgör E. *Polym. Eng. Sci.* 2004, 44, 1941–1948.
[30] Gao W, Zhou B, Ma X, Liu Y, Wang Z, Zhu Y. *Colloids Surf. A* 2011, 385, 181–187.
[31] Chen S, Hoffman S, Prots Y, Zhao JT, Kniep R. *Z. Anorg. Allg. Chem.* 2010, 636, 1710–1715.
[32] Ge C, Ding P, Shi L, Fu J. *J. Polym. Sci. Part B: Polym. Phys.* 2009, 47, 655–668.
[33] Wang Y, Liu W, Zhang H. *Polym. Test.* 2009, 28, 402–411.
[34] Wagener R, Reisinger TJG. *Polymer* 2003, 44, 7513–7518.
[35] Lai B, Ni X. *J. Macromol. Sci. Part B: Phys.* 2008, 47, 1028–1038.
[36] Sánchez-Solís A, Romero-Ibarra I, Estrada MR, Calderas F, Manero O. *Polym. Eng. Sci.* 2004, 44, 1094–1102.
[37] Olhero SM, Ferreira JMF. *Powder Technol.* 2004, 139, 69–75.
[38] Okada K, Mitsunaga T, Nagase Y. *Korea-Aust. Rheol. J.* 2003, 15, 43–50.
[39] Ren J, Silva AS, Krishnamoorti R. *Macromolecules* 2000, 33, 3739–3746.